Original Research Paper

Oxidation-strengthened disulfide-bridged prodrug nanoplatforms with cascade facilitated drug release for synergetic photochemotherapy

Bin Yang [a,d,1], Lin Wei [b,c,1], Yuequan Wang [a], Na Li [a], Bin Ji [d], Kaiyuan Wang [a], Xuanbo Zhang [a], Shenwu Zhang [a], Shuang Zhou [a], Xiaohui Yao [a], Hang Song [a], Yusheng Wu [d], Haotian Zhang [e], Qiming Kan [e], Tao Jin [b,f,**], Jin Sun [a,*]

[a] Wuya College of Innovation, Shenyang Pharmaceutical University, Shenyang 110016, China
[b] Ministry of Education, Heilongjiang University, Harbin 150500, China
[c] Sino-Russian Joint Graduate School, Heilongjiang University, Harbin 150080, China
[d] Department of Laboratory Medicine, The First Affiliated Hospital, China Medical University, Shenyang 110001, China
[e] School of Life Science and Biopharmaceutics, Shenyang Pharmaceutical University, Shenyang 110016, China
[f] School of Life Sciences, Heilongjiang University, Harbin 150080, China

ARTICLE INFO

ABSTRACT

One of the major barriers in utilizing prodrug nanocarriers for cancer therapy is the slow release of parent drug in tumors. Tumor cells generally display the higher oxidative level than normal cells, and also displayed the heterogeneity in terms of redox homeostasis level. We previously found that the disulfide bond-linkage demonstrates surprising oxidation-sensitivity to form the hydrophilic sulfoxide and sulphone groups. Herein, we develop oxidation-strengthened prodrug nanosystem loaded with pyropheophorbide a (PPa) to achieve light-activatable cascade drug release and enhance therapeutic efficacy. The disulfide bond-driven prodrug nanosystems not only respond to the redox-heterogeneity in tumor, but also respond to the exogenous oxidant (singlet oxygen) elicited by photosensitizers. Once the prodrug nanoparticles (NPs) are activated under irradiation, they would undergo an oxidative self-strengthened process, resulting in a facilitated drug cascade release. The IC_{50} value of the PPa@PTX-S-S NPs without irradiation was 2-fold higher than those of NPs plus irradiation. *In vivo*, the PPa@PTX prodrug NPs display prolonged systemic circulation and increased accumulation in tumor site. The PPa@PTX-S-S NPs showed much higher efficiency than free PTX or the PPa@PTX-C-C NPs to suppress the growth of 4T1 tumors. Therefore, this novel oxidation-strengthened disulfide-bridged prodrug-nanosystem has a great potential in the enhanced efficacy of cancer synergetic photochemotherapy.

* Corresponding author. Wuya College of Innovation, Shenyang Pharmaceutical University, No. 103, Wenhua Road, Shenyang 110016, China. Tel.: +86 24 23986325.
** Corresponding author. Ministry of Education, Heilongjiang University, Harbin 150500, China. Tel.: +86 24 23986320.
E-mail addresses: jintaoliu8@163.com (T. Jin), sunjin@syphu.edu.cn (J. Sun).
[1] Both contributed to this work equally.
Peer review under responsibility of Shenyang Pharmaceutical University.

1.   Introduction

Nowadays the incidence of breast cancer ranks first among female malignant tumors in China, so it is particularly important to achieve treatment for breast cancer and prevent recurrence [1].The most common treatment currently used in clinical trials is chemotherapy, which has significant effects but still has many serious side effects, including high toxicity and poor tumor selectivity [2,3]. With the rapid advances of nanotechnology and biomaterials, nanoparticle drug delivery systems (nano-DDSs) have captured the vision, especially smart self-assembling prodrug nanoparticles, which combine prodrug strategies with nano-DDS owing to their prominent strengths such as good stability, high drug-loading ratio, favorable anti-crystallization and extended circulation time in blood [4–6]. Even so, there are still some obstacles in the prodrug-based nanoparticles, which need to release the parent drug on-demand to take effect in the tumor site.

There are increased glutathione (GSH) and reactive oxygen species (ROS)levels in tumor cells in comparisons with normal cells, resulting in the high redox micro-environment in tumor, which inspires us to rationally design prodrug nano-DDS [7–9]. However, the tumor cells have the specific redox heterogeneity, indicating that there exists relatively large different levels of GSH and ROS regardless of the diverse stages of tumors or disparate regions of the same tumor cell, which makes it of great tough to release parent drug on time [10–12]. In addition, photodynamic therapy (PDT) has gained striking progresses in the clinical cancer treatment and has even been approved by FDA for the low toxicity of photosensitizer (PS) and the inoffensive light irradiation [13,14]. Furthermore, the PS-encapsulated prodrug nanoparticles (NPs) could effectively generate more singlet oxygen ($^1O_2$) within tumor sites under near infrared (NIR) light irradiation to induce apoptosis and then the produced ROS could further cleave the chemical bond which is sensitive to oxidation, in order to on demand discharge the active parent drug [15,16]. Surprisingly, we recently demonstrated that disulfide bonds are responsive not only to the reductive condition, but also to the oxidative condition to form the hydrophilic sulfoxide and sulphone groups [17,18].

Based on the above findings, we herein intend to design a new oxidation-strengthened disulfide bond-driven prodrug nanomedicine containing a photosensitizer, hoping to combine chemotherapy and photodynamic therapy to on-demand release the active parent drugs in tumors. We construct a self-assembled PPa-encapsulated prodrug nanoparticles based on the disulfide bond-linkage conjugate of paclitaxel (PTX) and oleic acid (OA), with carbon-carbon linkage as a negative control. The novel nanoparticles could synergistically combine chemotherapy and phototherapy and also show high anticancer efficacy in the treatment of breast cancers for its dual-source ROS-triggered PTX release (Fig. 1).

2.   Materials and methods

2.1.   Materials

The PTX prodrugs (PTX-S-S-OA and PTX-C-C-OA) were offered by colleagues in our group. Pyropheophorbide a (PPa) was purchased from Shanghai Dibai Bio-Technology Co, Ltd. (Shanghai, China). 1, 2-distearoyl-sn-glycero-3-phosphoethanolamine-N- [methoxy(polyethyleneglycol)-2000] (DSPE-PEG$_{2k}$) was purchased from Shanghai Advanced Vehicle Technology LTD (Shanghai, China). MTT was purchased from Sigma Aldrich (Shanghai, China) Trading Co., Ltd. (Shanghai, China). Hochest was obtained from Vector Laboratories (Burlingame, CA). All cell-culture related reagents were obtained from GIBICO, Invitrogen Corp. (Carlsbad, CA).

2.2.   Preparation of paclitaxel prodrug nanoparticles

The PPa@PTX-S-S-OA/DSPE-PEG$_{2k}$ NPs were prepared exquisitely by one-step nanoprecipitation method [5,19]. In brief, 2 mg of PTX-S-S-OA and 0.4mg of DSPE-PEGS$_{2k}$ were dissolved in 0.3ml ethanol, and 100 μl of PPa solution was added into the above mixture. The PPa solution was of the concentration of 1mg/ml with the solvent tetrahydrofuran (THF). The mixed organic solution was slowly added into 2 ml deionized water under stirring at 800 r/min. After that, the organic solution in the formulation was removed by rotary evaporators at room temperature. The final formulation was diluted with deionized water to 2 ml. And now, we get the PPa@PTX-S-S-OA/DSPE-PEG$_{2k}$ NPs of the concentration of 1mg/ml. In addition, the PPa@PTX-C-C-OA/DSPE-PEG$_{2k}$ was prepared with the similar method mentioned above, except the fact that the PTX-S-S-OA prodrug was replaced with PTX-C-C-OA. The prepared PPa@PTX-S-S-OA/DSPE-PEGS$_{2k}$ NPs and PPa@PTX-C-C-OA/ DSPE-PEG$_{2k}$ NPs (below described as PPa@PTX-S-S NPs and PPa@PTX-C-C NPs for short.) were stored at 4 °C for the next experiments.

2.3.   Characterization of the paclitaxel prodrug NPs

Dynamic light scattering (DLS) (Zetasizer Nano ZS, Malvern Co. UK) was conducted for measuring the paclitaxel prodrug nanoparticles. The morphology of PPa@paclitaxel prodrug nanoparticles was analyzed by transmission electron microscope (TEM) (JEOL 100CX II, Japan). The drug loading and encapsulation efficiency of PPa@paclitaxel prodrug nanoparticles were detected by HPLC. In addition, the PPa@PTX prodrug nanoparticles were added into PBS (pH 7.4) solution containing with 10% FBS at 37 °C for 48h. The particle size of nanoparticles was measured at preset time intervals using DLS to determine the colloidal stability. Furthermore, the long-term storage ability at 4 °C for nanoparticles was also examined by DLS using the change of particle size as an indicator for 3 months.
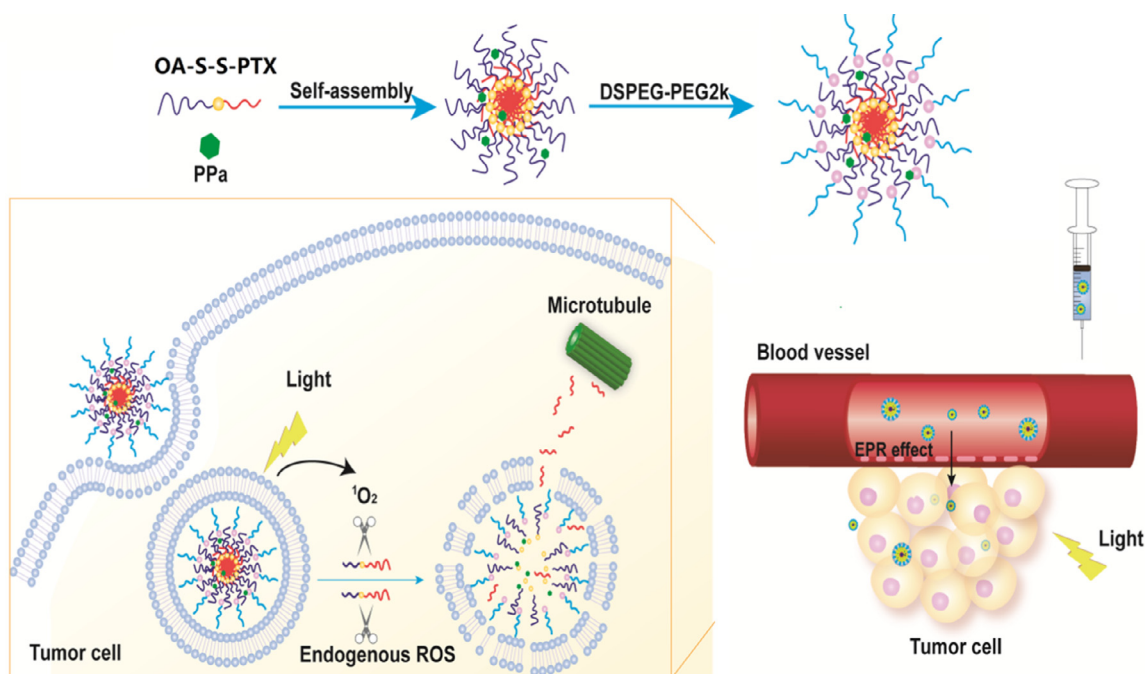
Fig. 1 – Schematic illustration of disulfide bond-driven prodrug NPs displayed light-activated fast drug release and chemo-photodynamic therapy.

2.4. In vitro release of PTX from prodrug NPs

To investigate the PTX release behavior from PPa@S-S NPs and PPa@C-C NPs under different circumstances, the prodrug NPs were suspended in the media of PBS buffer (pH 7.4) containing with 30% ethanol (30 ml) for use. And then we explore whether the extra H_2O_2 or Near Infrared light could trigger PTX release from the nanoparticles.

Firstly, we study the H_2O_2-triggered test group, each media was added extra H_2O_2 of 0 2, 5, 10 mM, respectively. Afterwards, 0.2 ml media was taken out at predetermined time intervals for HPLC to analyze the PTX release behavior at 227 nm. Similarly, each media was irradiated with 660 nm light (0.25 w/cm^2) for 0, 2, 5, 10 min respectively for the NIR light-triggered test groups. And HPLC was also used to record PTX release condition. Besides, we also examined the groups that treated by 5mM H_2O_2 and 660 nm light irradiation for 10 min. All the experiments were carried out in triplicate and the results are expressed as mean $\pm$ SD (n=3).

2.5. Cellular uptake

4T1 cancer cells were the optimal pick as well for the cellular uptake experiments. The cell slides were preset into the 12-well plates before 4T1 cells were seeded (1.0×10^5 cells/well) and incubated at 37 °C for 24 h. Subsequently, the cells were involved with the media containing with PPa and PPa@paclitaxel prodrug NPs with equivalent concentration of PPa (3 μg/ml) and proceed with incubation at 37 °C for 0.5 h and 2 h. After that, the media was suck out and then flushed 3 times with cold PBS (pH 7.4). And then 4% paraformaldehyde

was employed for fixation (15 min) and followed by 3 times flush with cold PBS (pH 7.4). Eventually, Hochest was carried out for the nuclei counter stained (10 min) and the cold PBS was also used to wash 3 times. Confocal laser scanning microscopy (Zeiss LSM 510 Meta, Germany) was used for monitoring fluorescence intensity of PPa@paclitaxel prodrug NPs.

For the Flow Cytometry experiment, 4T1 cells were pre-seeded onto 24-well plates(1.0×10^5 cells/well) and incubated for 24 h before the cells were treated with the media involved with PPa, PPa@paclitaxel prodrug nanoparticles as well as non treated cells as control and then carried on incubation for 0.5 h and 2 h at 37 °C. After that, the media was abandoned accompanied with 3 times washing by cold PBS (pH7.4). And then the cells were digested with trypsin (0.5 ml) for 7 min, collected and resuspended in fresh RPMI-1640 media (0.4 ml) to end the digestion. Later, the cells were centrifuged for 5 min under 3000 r/min and discarded supernatant, while the harvested cells were resuspended with PBS (0.3 ml) and prepared to monitor the cellular uptake intensity through Flow Cytometry (FACS Calibur, BD Biosciences, San Jose, CA).

2.6. Intracellular generation of ROS

To study intracellular ROS generation, 4T1 cells were pre-seeded onto 24-well plates (1.0×10^5 cells/well) and incubated for 24h. After that, the media was replaced with fresh 1640 media containing PPa and PPa@paclitaxel NPs and incubated at 37 °C for another 3 h. The fluorescence probe of ROS (DCFH-DA) was then added and irradiated by 660 nm light (60 mw/cm^2) for 1min after incubation for 0.5 h. Eventually, the

green fluorescence of reactive oxygen species was detected by fluorescent microscopy.

2.7. Cell viability studies

The *in vitro* cellular experiments were valuated against 4T1 cells (murine breast cells) that purchased from American Type Culture Collection (ATCC) and cultured under standard protocols (37 °C, 5% humidity of CO_2).

For the cytotoxicity test, 4T1 cells were pre-seeded onto 96-well plates (1.0×10^3 cells/well) and incubated for 24h till the most of cells have attached to the plates. After that, the old media was replaced by fresh RPMI-1640 media involved with PTX, PPa and PPa@ paclitaxel prodrug NPs with diverse concentration. After incubation for 4 h, one group of cells was treated with direct irradiation by 660 nm light (60 mw/cm^2) for 8 min, while the other group remained incubation. The MTT assay was conducted according to the protocol after continuing incubation for 48 and 72 h with Microplate reader. All the results were carried out in triplicate as well as three independent tests.

2.8. Ex vivo biodistribution

The bio-distribution experiment was performed using 4T1 murine breast cells as the tumor xenograft models. Firstly, 4T1 cells together with 5% PBS solution were harvested and subcutaneously grafted at the right back of the mice (1.0×10^6). And after the tumor volume gradually grew to 500 mm^3, the tumor bearing mice were divided into 3 groups at random(9 for each group) and intravenously injected free PPa and PPa@paclitaxel NPs, respectively ($n=3$, the equivalent doses of PPa: 2 mg/kg) via the tail. At present time intervals (4, 12, 24 h) post-injection, all the mice were sacrificed and dissected to get the vital organs such as: heart, liver, spleen, lung, kidney and tumor. *IVIS* spectrum small-animal imaging system was utilized to analyze the *ex vivo* distribution of these nanoparticles.

2.9. In vivo antitumor efficacy

All the live animal experiments were conducted in compliance with the protocols of Shenyang Pharmaceutical University and animal care institution. All the female BALB/C mice provided were from Animal Center of Shenyang Pharmaceutical University and fostered under suitable conditions.

All the female BALB/C mice bearing 4T1 cells were randomly allocated into 9 groups ($n=6$) when the tumor volume grew to 100–150 mm^3. Meanwhile, the formulations below were respectively i.v. administered through the mice tail vein every other day. PBS (a), PTX (b), PPa (c), PPa@PTX-C-C NPs (d, e) and PPa@PTX-S-S NPs (f, g). And 660 nm light irradiation (0.2 w/cm^2, 8 min) was employed for c, d and f groups after 12 h post-injection. Every day morning we weighed the mice and measured the tumor volume by using a caliper and then calculated and recorded the tumor growth with the formula below: tumor volume

$=$ length $\times$ width $\times$ width/2. All the mice were killed and dissected after the fifth irradiation and the integrated tumor sections were taken out, weighed and took the picture. The other organs in each group were also collected (heart, liver, spleen, lung, and kidney), fixated with 4% paraformaldehyde and to be prepared for H&E staining experiment.

3. Results and discussion

3.1. Preparation and characterization of PPa@ PTX prodrug NPs

The PPa@PTX prodrug nanoparticles were fabricated by one-step simple nano-precipitation method that PPa and PTX prodrug molecules could spontaneously assemble together prior to precipitation as they come across [5,6]. As shown in Fig. 2A and 2B, we could observe that both PPa@PTX prodrug NPs have nearly spherical structures with narrow-distribution particle size. Table S1 showed that average diameters of PPa@PTX-S-S NPs and PPa@PTX-C-C NPs were 78.2 ± 2.4 and 80.8 ± 3.0 nm with small Polydispersity index (PDI) of 0.11 ± 0.03 and 0.12 ± 0.02 by DLS, respectively. To the best of our knowledge, the small-sized nanoparticles (less than 100 nm) maybe displayed the superior ability to accumulate in tumor site by the passive enhanced permeability and retention effect.

The zeta potentials of two PPa@PTX prodrug NPs were about negative 20 mV, indicating that the prodrug nanoparticles have stable colloidal dispersion and low elimination capability by liver *in vivo*. It was further testified by the colloidal stable experiment (Fig. 2C). In addition, the two PPa @PTX prodrug NPs were also stable at 4 °C for 90 d (Fig. 2D). The PPa@PTX-C-C NPs and PPa@PTX-S-S NPs provided the entrapment efficacy for PPa of 79.7% and 90.2%, respectively. In addition, the drug loading content of the PPa@PTX-C-C NPs and PPa@PTX-S-S NPs 60.7% and 63.5%, respectively, which were far more improved than the traditional nano-drugs (less than 10%).

3.2. In vitro release of PTX from PPa@PTX prodrug NPs

In order to explore the release mechanism of PTX from PPa@PTX prodrug NPs, the inspection of *in vitro* release behavior was carried out and verified if the extra ROS or light irradiation could trigger more PTX release from the prodrug NPs. Firstly, PPa@PTX-S-S NPs and PPa@PTX-C-C NPs were treated with different concentrations of H_2O_2 (0, 2, 5 and 10 mM), respectively. Fig. 3A–B showed that PPa@PTX-C-C NPs hardly released PTX within 12 h even with 10 mM H_2O_2, while PPa@PTX-S-S NPs released more than 70% in 12 h with 10 mM H_2O_2, indicating that the disulfide bond in PPa@PTX-S-S NPs displayed great oxidative sensitivity to facilitate PTX release. And then we assessed the effect of 660 nm laser irradiation on PTX release. As shown in Fig. 3C and 3D, the release rate of PTX was significantly faster in the first 4 h after irradiation at 660 nm, indicating that PTX-S-S-OA were a light-activatable prodrug. The reason might be that PPA is
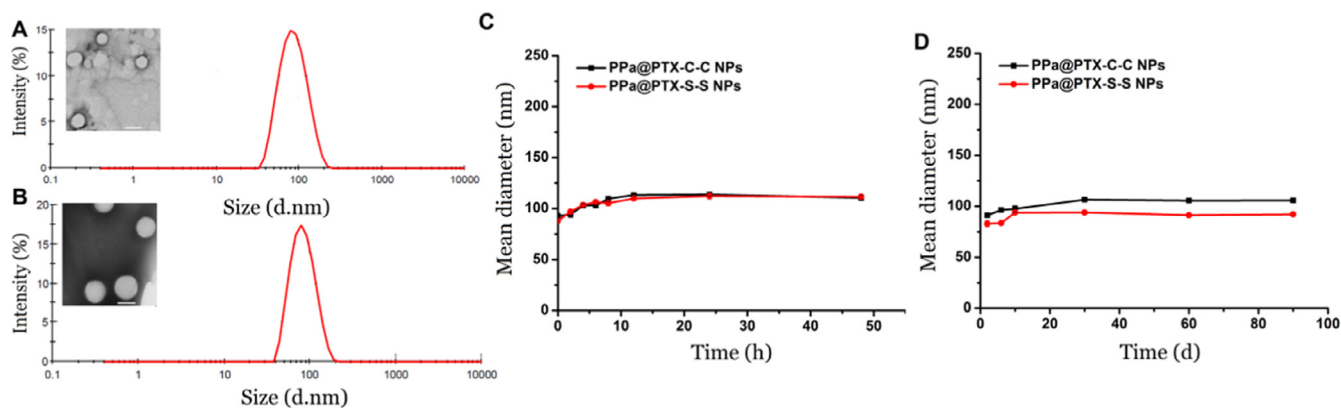
Fig. 2 – TEM image and DLS results of (A) PPa@PTX-C-C NPs and (B) PPa @PTX-S-S NPs(scale bar 100 nm). (C) Colloidal stability of PPa@PTX-S-S NPs and PPa@PTX-C-C NPs after incubation in PBS (pH 7.4) supplemented with 10% FBS at 37 °C. (D) Long-term stability of PPa@PTX-S-S NPs and PPa@PTX-C-C NPs after store at 4 °C.
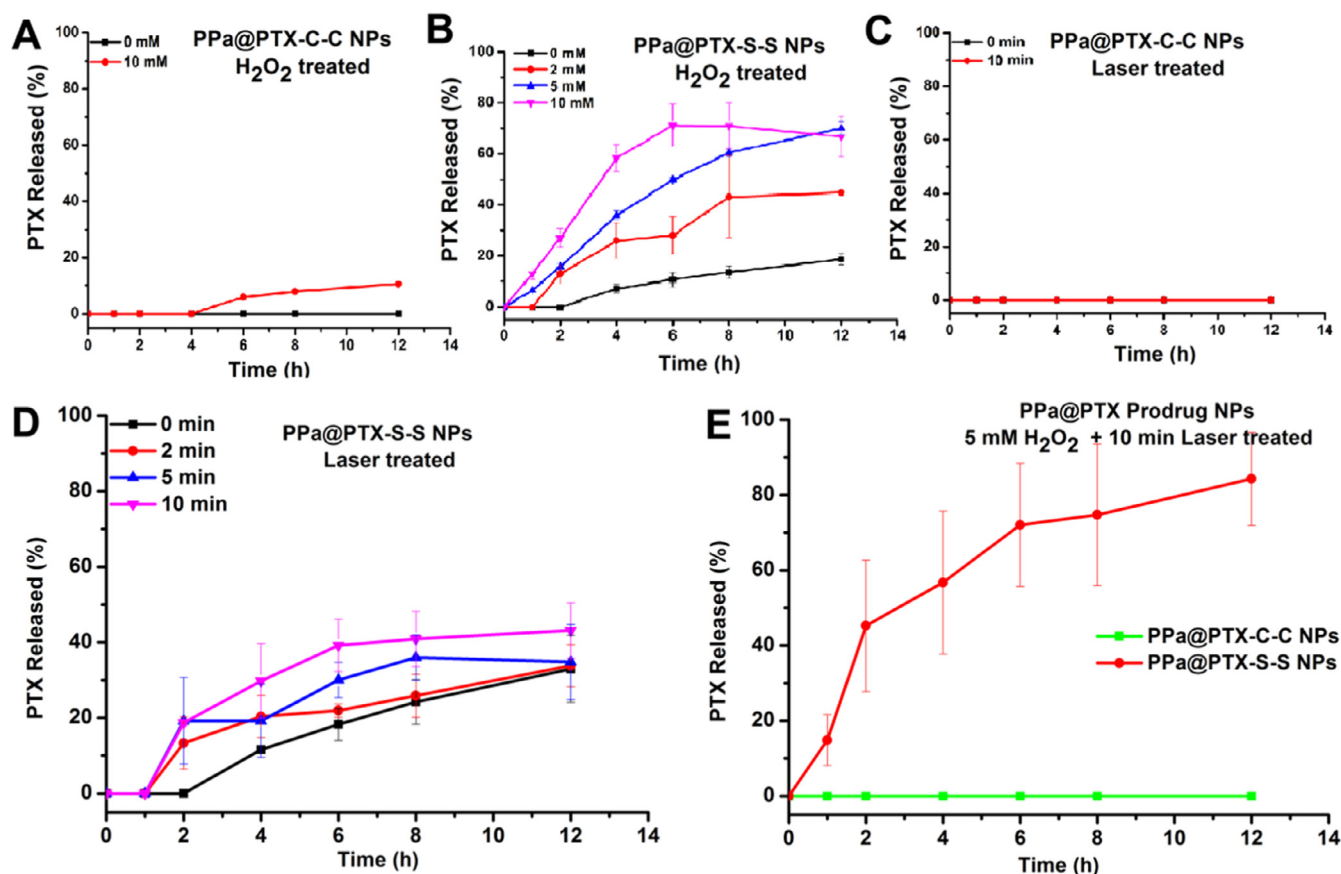

Fig. 3 – PTX release from PPa@PTX-C-C NPs (A) or PPa@PTX-C-C NPs (B) in the presence of various concentrations of H_2O_2. ($n = 3$);PTX release from PPa@PTX-C-C NPs (C) or PPa@PTX-C-C NPs (D) with 660 nm wavelength laser irradiation for different times; ($n = 3$); (E) PTX release from PPa@PTX-C-C NPs (C) or PPa@PTX-C-C with H_2O_2 and laser.

encapsulated in nanoparticles, and exogenous ROS can be produced by irradiation at 660 nm to trigger the oxidation of prodrug [20].

To further investigate the effects of endogenous ROS in combination with exogenous ROS, we explored the PPa@PTX NPs group treated by 5 mM H_2O_2 plus 10 min irradiation. Fig. 3E showed that PPa@PTX-S-S NPs released approximately

50% within 2 h and reached over 80% in 4 h, higher than H_2O_2-treated group or 660 nm irradiation test group solely, whereas, PPa@PTX-C-C NPs group did not release PTX, indicating that endogenous ROS, in combination with exogenous ROS triggered by 660 nm irradiation, could synergistically promote PTX release. The results of *in vitro* release confirmed that the disulfide bond in PPa@PTX-S-
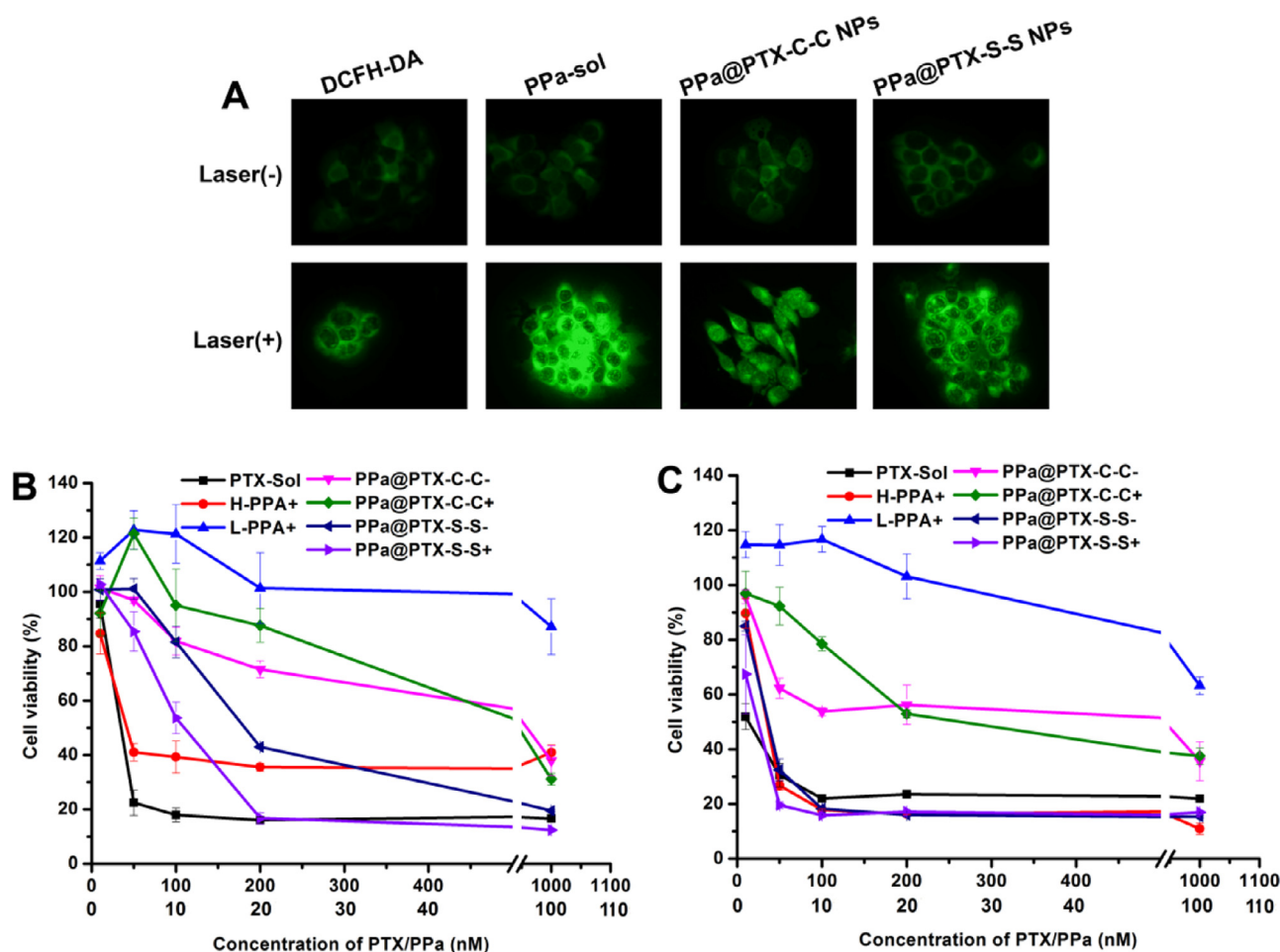
Fig. 4 – (A) Fluorescence intensity of DCFH determining the concentration of ROS using fluorescence microscopy, the formulations contain an equivalent concentration of PPa (20 nM). Images of 4T1 breast cancer cells incubated with PPa-sol or PPa@prodrug NPs with irradiation (+) or not (–). *In vitro* cytotoxicities of different concentrations of PTX-sol, free PPa and PPa@prodrug NPs toward 4T1 cancer cells incubated for (B) 48 h and (C) 72 h. HPPa represents the concentration of PPa equivalent to the PTX.

S NPs showed a strong responsiveness to endogenous and exogenous ROS. More importantly, once the PPa@PTX-S-S NPs were activated under irradiation, they would be more sensitive to the H_2O_2, leading to a facilitated cascade drug release [21].

3.3. Cellular uptake

The cellular uptake experiment was carried out in 4T1 cells of free PPa and PPa@PTX NPs within 0.5 h and 2 h. As shown in Fig. S1A and S1B, PPa (red) can be easily found in all the cells, indicating that PPa@PTX NPs have been effectively taken up in 4T1 cells among the others in 0.5 h and 2 h. What's more, the uptake amount of 4T1 cells was time-dependent.

In addition, we further investigated the quantitative cellular uptake by flow cytometry. As seen in Fig. S1C, the fluorescent intensity of PPa@PTX NPs was significantly higher than the others, and the fluorescence in 2 h was

obviously bigger than that in 0.5 h, similar to the above results.

3.4. Intracellular ROS detection

We determined the change in intracellular ROS level with or without 660 nm irradiation by DCFH-DA method (a fluorescent probe of ROS). The groups treated without irradiation were designed as a control. As shown in Fig. 4A, the groups treated without irradiation showed a clearly fluorescence, indicating a certain amount of ROS in tumor cells. What's more, we could obviously notice that the ROS level in the 660 irradiation treated groups was obviously much higher than that of the non-treated groups, which actually proved that PPa@PTX NPs indeed generate high ROS level under irradiation [16,22].

3.5. Cell viability studies

In vitro cytotoxicity of 4T1 cells was assessed by using the MTT assay. As shown in Fig. 4B and 4C, the PPa@PTX-C-C
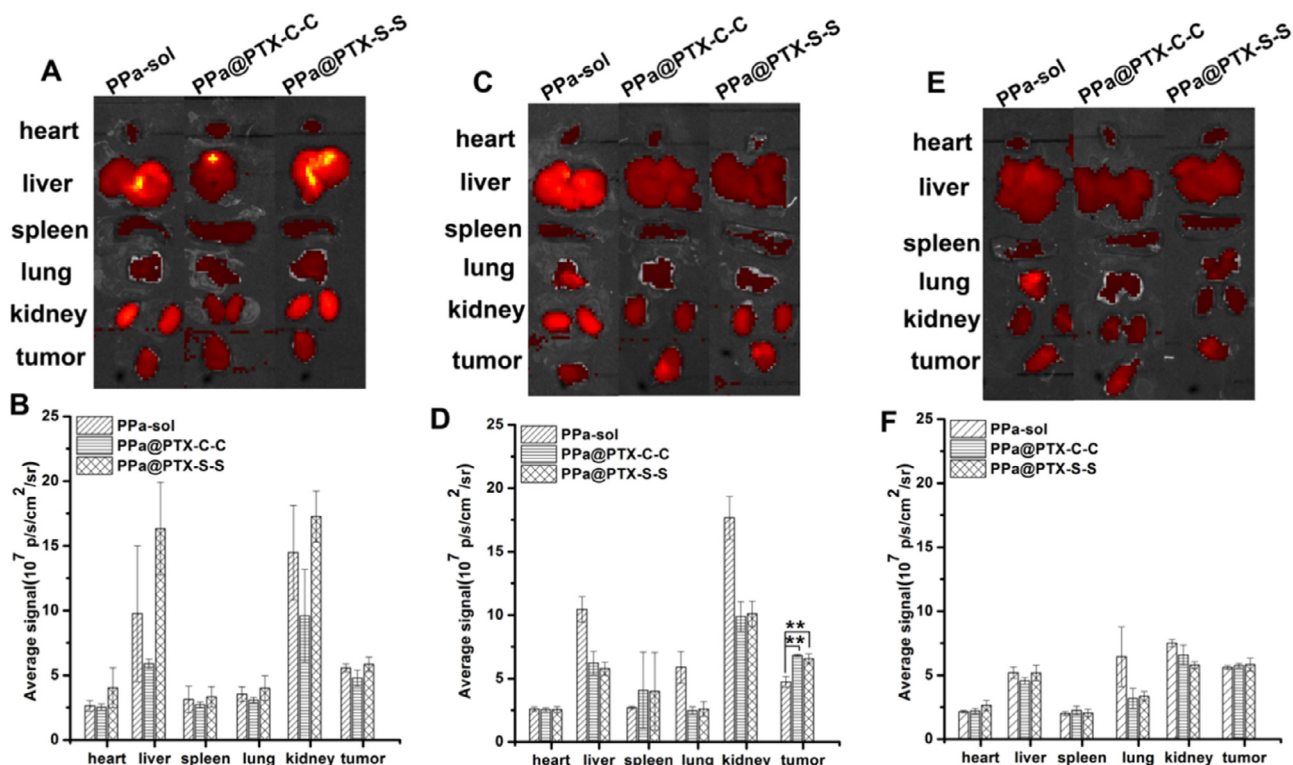
Fig. 5 – *Ex vivo* fluorescence images of major organs after injection of PPa-sol, PPa@PTX-C-C or PPa@PTX-S-S for (A) 4 h, (C) 12 h and (E) 24 h; semi-quantitative biodistribution of PPa-sol, PPa@PTX-C-C or PPa@PTX-S-S determined by the average PPa fluorescence intensity of organs post-injection for (B) 4 h, (D) 12 h and (F) 24 h. The data are shown as mean ± SD (n = 3).

group showed negligible cytotoxicity both under light and in the dark, while the PPa@PTX-S-S group exhibited obvious cytotoxicity, indicating that endogenous ROS could activate the disulfide bond to promote PTX release. Surprisingly, cell viability of the PPa@PTX-S-S group without light irradiation was around two times higher than their corresponding NPs plus laser at low concentrations (Table S2), indicating that disulfide bond also showed a good responsiveness to exogenous ROS produced by PDT. These above results were in consistent with the *in vitro* release study, indicating that the disulfide bond could be activated by both endogenous and exogenous ROS to rapidly release the parent active drug PTX.

3.6. Ex vivo bio-distribution

The tumor bearing mice were applied to study the biodistribution performance of PPa solution and PPa@PTX prodrug NPs. After intravenous injection at certain time points, the mice were killed and the vital organs were taken out for *IVIS* small-animal imaging system at pre-set time (4, 12 and 24 h). As shown in Fig. 5, the fluorescence intensity of PPa-sol was higher than that of the PPa@PTX prodrug NPs, mainly in the liver and kidney after 12 h of administration, while the fluorescence intensity of the PPa@PTX prodrug NPs at the tumor site was significantly higher than that of PPa-sol. What's more, the florescence intensity in tumor for both PPa@PTX-C-C NPs and PPa@PTX-S-S NPs groups continuously increased and reached the maximum at 12 h, the high accumulation of which might be due to the long *in*

vivo circulation of nanoparticles in blood [23–25]. Even though the fluorescence of PPa@PTX prodrug NPs at the tumor site was slightly decreased at 24 h, this would not influence later antitumor treatment. Because the PPa@PTX prodrug NPs were activated by light, they became more sensitive to reactive oxygen species, so the reactive oxygen species in the tumor cells would accelerate the release of the PTX, which have been validated by the above *in vitro* release experiments.

3.7. In vivo anti-tumor efficacy

For the *in vivo* anti-tumor efficacy experiment, 4T1 tumor-bearing mice were randomly divided into 7 groups (n=6) and equal formulations (6 mg/kg doses of PTX equivalent concentration, 100 μl) were given intravenously via the tail vein every other day for five times, accompanied with 660 nm irradiation (0.2 w/cm^2, 8 min) for PPa, PPa@PTX-C-C NPs and PPa@PTX-S-S NPs groups at 12 h post-injection. The tumor volume and body weight of tumor-bearing mice were daily measured and recorded to draw the grow curves in Fig. 6A and 6B. As shown in Fig. 6A, PPa-sol with 660 nm irradiation treated slightly suppress tumor growth, manifesting PDT alone made little influence in the antitumor effect. As for the similar poor anti-tumor efficacy of PPa@PTX-C-C NPs+ and PPa@PTX-C-C NPs- groups, the redox micro-environment in tumor even together with the produced ROS by irradiation barely cleaved C-C bond to release PTX. However, PPa@PTX-S-S NPs exhibited obvious anti-tumor efficacy among the others, especially PPa@PTX-S-S NPs+ that almost inhibited tumor
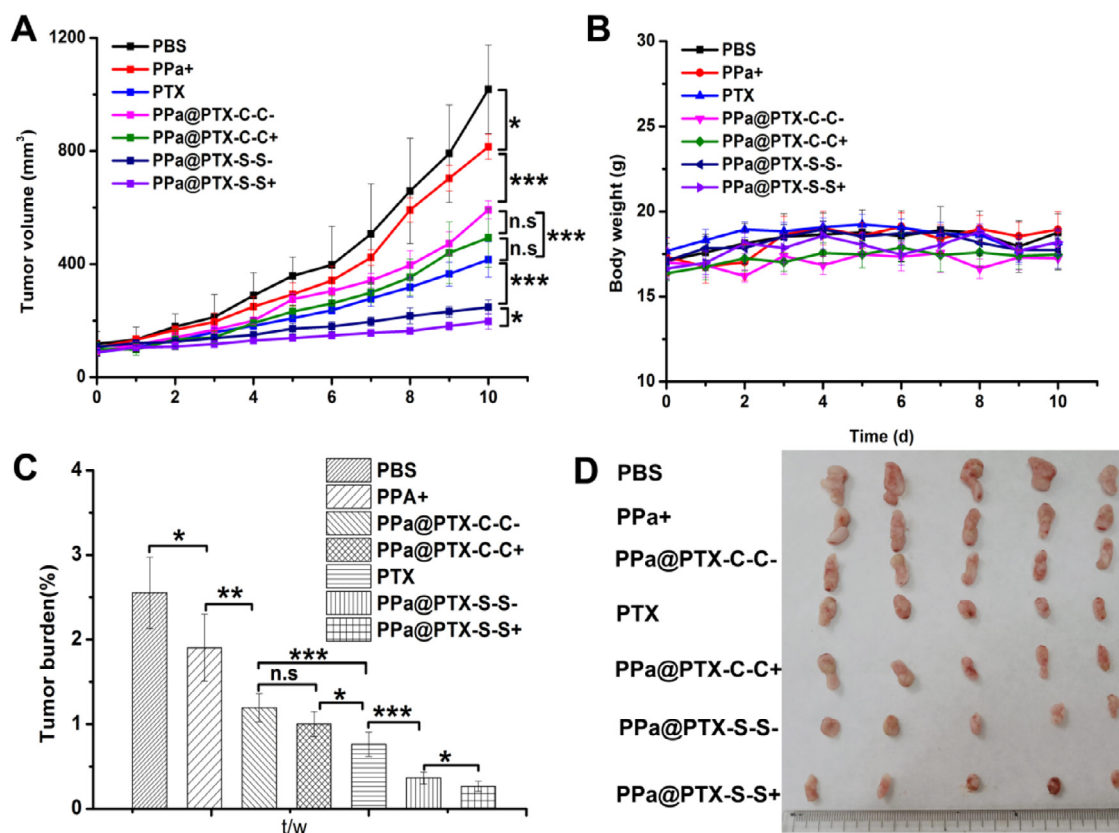
Fig. 6 – *In vivo* antitumor effect in 4T1 tumor bearing mice. (A) The tumor growth curves of mice treated with different formulations. (B) The body weights of different groups after various treatments. (C) Tumor burden after the last treatment. (D) Images of tumors after the last treatment. The data are shown as mean ± SD (n = 5), *P < 0.05. **P < 0.01, and ***P < 0.001.

growth efficiently. Such excited results, we speculated, may result from the following reasons. Firstly, the high endogenous ROS levels provided by tumor itself made PPa@PTX NPs easily tell tumor cells from normal cells, thus enhancing the selective PTX release from NPs [26,27]. Secondly, the encapsulated PPa could generate more ROS ($^1O_2$) under irradiation to cleave redox-sensitive linkages such as, S-S bond and then rapidly on-demand release PTX, which has united chemo-therapy and PDT, furnishing a better solution in cancer therapy. Thirdly, the PPa@PTX NPs exhibited a prolonged circulation time, and avoided the quick elimination, thus guaranteeing reliable tumor accumulation [28,29].

In Fig. 6B, we've also drawn a body weight-time chart and none of the groups appeared to sharply change for 10 d, indicating all the formulations used have good safety. We still conducted H&E staining test to verify other possible side-effects [30,31]. From Fig. S2, we could notice that all the organs were in good condition, except the livers in group (a) and (b) have slight damages, demonstrating our NPs were safe with no obvious side-effects.

4. Conclusion

In this work, we have designed a smart prodrug nanosystem to probe the oxidative responsiveness of disulfide bond and the synergistic chemo-photodynamic therapy for breast cancer. The prodrug nanosystems containing disulfide

bond showed oxidative responsiveness in terms of both endogenous and exogenous ROS, and displayed good stability, high drug-loading ratio, extended circulation time in blood and enhanced accumulation in tumor site. Different from traditional understanding, disulfide bonds were activated by high GSH levels in tumor sites to achieve rapid release of drugs. In this study, the prodrug nanosystems containing disulfide bond could realize chemo-photodynamic therapy in response to the endogenous and endogenous ROS concentration, leading to an obvious cytotoxicity in cancer cells and high-efficiency antitumor effect. What's more, it is the first example of a disulfide bond-linkage prodrug NPs combined with PDT to accelerate the release of the active parent drug. This novel oxidation-strengthened disulfide-bridged prodrug-nanosystem has a great potential in the enhanced efficacy of cancer synergetic photochemotherapy.

Conflicts of interest

The authors declare no competing financial interest.

Acknowledgments

Supplementary materials

Supplementary material associated with this article can be found, in the online version, at doi:10.1016/j.ajps.2019.09.001.

REFERENCES

[1] Chen MC, Lee KD, Lu CH, Wang TY, Huang SH, Chen CY. The bidirectional association among female hormone-related cancers: breast, ovary, and uterine corpus. Cancer Med-US 2018;7:2299–306.

[2] Wheate NJ, Walker S, Craig GE, Oun R. The status of platinum anticancer drugs in the clinic and in clinical trials. Dalton Trans 2010;39:8113–27.

[3] Smith RA, Andrews KS, Brooks D, Fedewa SA, Manassaram-Baptiste D, Saslow D, et al. Cancer screening in the united states, 2017: a review of current american cancer society guidelines and current issues in cancer screening. CA Cancer J Clin 2017;67:100–21.

[4] Luo C, Sun J, Sun B, He Z. Prodrug-based nanoparticulate drug delivery strategies for cancer therapy. Trends Pharmacol Sci 2014;35:556–66.

[5] Wang Y, Liu D, Zheng Q, Zhao Q, Zhang H, Ma Y, et al. Disulfide bond bridge insertion turns hydrophobic anticancer prodrugs into self-assembled nanomedicines. Nano Lett 2014;14:5577–83.

[6] Luo C, Sun J, Liu D, Sun B, Miao L, Musetti S, et al. Self-assembled redox dual-responsive prodrug-nanosystem formed by single thioether-bridged paclitaxel-fatty acid conjugate for cancer chemotherapy. Nano Lett 2016;16:5401–8.

[7] Stehle G, Sinn H, Wunder A, Schrenk HH, Stewart JC, Hartung G, et al. Plasma protein (albumin) catabolism by the tumor itself–implications for tumor metabolism and the genesis of cachexia. Crit Rev Oncol Hemat 1997;26:77–100.

[8] Mohamed MM, Sloane BF. Multifunctional enzymes in cancer. Nat Rev Cancer 2006;6:764–75.

[9] Sameni M, Moin K, Sloane BF. Imaging proteolysis by living human breast cancer cells. Neoplasia 2000;2:496–504.

[10] Lee FYF, Vessey A, Rofstad E, Siemann DW, Sutherland RM. Heterogeneity of glutathione content in human ovarian Cancer. Cancer Res 1989;49:5244.

[11] Fang J, Seki T, Maeda H. Therapeutic strategies by modulating oxygen stress in cancer and inflammation. Adv Drug Deliver Rev 2009;61:290–302.

[12] Grek CL, Tew KD. Redox metabolism and malignancy. Curr Opin Pharmacol 2010;10:362–8.

[13] Lucky SS, Soo KC, Zhang Y. Nanoparticles in photodynamic therapy. Chem Rev 2015;115:1990–2042.

[14] Boyle DG, Grindey GB, Weishaupt KR, Fiel R, Dougherty TJ. Photoradiation therapy. II. cure of animal tumors with hematoporphyrin and light. J Natl Cancer I 1975;55:115–21.

[15] Macdonald IJ, Dougherty TJ. Basic principles of photodynamic therapy. J Porphyr Phthalocya 2001;05:105–29.

[16] Yue C, Zhang C, Alfranca G, Yang Y, Jiang X, Yang Y, et al. Near-infrared light triggered ROS-activated theranostic platform based on ce6-cpt-ucnps for simultaneous fluorescence imaging and chemo-photodynamic combined therapy. Theranostics 2016;6:456–69.

[17] Sun B, Luo C, Yu H, Zhang X, Chen Q, Yang W, et al. Disulfide bond-driven oxidation- and reduction-responsive prodrug nanoassemblies for cancer therapy. Nano Lett 2018;18:3643–50.

[18] Zhang D, Yang J, Guan J, Yang B, Zhang S, Sun M, et al. *In vivo* tailor-made protein corona of a prodrug-based nanoassembly fabricated by redox dual-sensitive paclitaxel prodrug for the superselective treatment of breast cancer. Biomater Sci 2018;6:2360–74.

[19] Yang B, Wang K, Zhang D, Sun B, Ji B, Wei L, et al. Light-activatable dual-source ROS-responsive prodrug nanoplatform for synergistic chemo-photodynamic therapy. Biomater Sci 2018;6:2965–75.

[20] Yue C, Zhang C, Alfranca G, Yang Y, Jiang X, Yang Y, et al. Near-infrared light triggered ROS-activated theranostic platform based on Ce6-CPT-UCNPs for simultaneous fluorescence imaging and chemo-photodynamic combined therapy. Theranostics 2016;6:456–69.

[21] Gong H, Dong Z, Liu Y, Yin S, Cheng L, Xi W, et al. Engineering of multifunctional nano-micelles for combined photothermal and photodynamic therapy under the guidance of multimodal Imaging. Adv Funct Mater 2014;24:6492–502.

[22] Napoli A, Valentini M, Tirelli N, Müller M, Hubbell JA. Oxidation-responsive polymeric vesicles. Nat Mater 2004;3:183–9.

[23] Zhang W, Lin W, Pei Q, Hu X, Xie Z, Jing X. Redox-hypersensitive organic nanoparticles for selective treatment of cancer cells. Chem Mater 2016;28:4440–6.

[24] Zhou H, Fan Z, Deng J, Lemons PK, Arhontoulis DC, Bowne WB, et al. Hyaluronidase embedded in nanocarrier peg shell for enhanced tumor penetration and highly efficient antitumor efficacy. Nano Lett 2016;16:3268–77.

[25] Yang B, Wang K, Zhang D, Ji B, Zhao D, Wang X, et al. Polydopamine-modified ROS-responsive prodrug nanoplatform with enhanced stability for precise treatment of breast cancer. RSC Adv 2019;9:9260–9.

[26] Ye M, Han Y, Tang J, Piao Y, Liu X, Zhou Z, et al. A tumor-specific cascade amplification drug release nanoparticle for overcoming multidrug resistance in cancers. Adv Mater 2017;29:1702342.

[27] Shim MS, Xia Y. A reactive oxygen species (ros)-responsive polymer for safe, efficient, and targeted gene delivery in cancer cells. Angew Chem Int Edit 2013;52:6926–9.

[28] Tian J, Ding L, Xu HJ, Shen Z, Ju H, Jia L, et al. Cell-specific and pH-activatable rubyrin-loaded nanoparticles for highly selective near-infrared photodynamic therapy against cancer. J Am Cheml Soc 2013;135:18850–8.

[29] Pei Q, Hu X, Zheng X, Liu S, Li Y, Jing X, et al. Light-activatable red blood cell membrane-camouflaged dimeric prodrug nanoparticles for synergistic photodynamic/chemotherapy. ACS Nano 2018;12:1630–41.

[30] Yang B, Ai X, Shang L, Zhong L, Ji B, Wu C, et al. Doxorubicin-loaded redox-responsive polymeric nanomicelles delivery system to reverse multidrug resistance in drug-resistant breast cancer cells. J Nanosci Nanotechno 2016;16:8424–30.

[31] Wong HL, Bendayan R, Rauth AM, Li Y, Wu XY. Chemotherapy with anticancer drugs encapsulated in solid lipid nanoparticles. Adv Drug Deliver Rev 2007;59:491–504.